Rod Outer Segment Structure Influences The Apparent Kinetic Parameters of Cyclic GMP Phosphodiesterase

CHARLES L. DUMKE,* VADIM Y. ARSHAVSKY,* PETER D. CALVERT,*‡ M. DERIC BOWNDS,*‡§ and EDWARD N. PUGH, JR‖

From the *Bock Laboratories ‡Neuroscience Training Program and the §Department of Zoology, University of Wisconsin, Madison, Wisconsin 53706; and ‖Department of Psychology and Institute of Neurological Sciences, University of Pennsylvania, Philadelphia, Pennsylvania

ABSTRACT Cyclic GMP hydrolysis by the phosphodiesterase (PDE) of retinal rod outer segments (ROS) is a key amplification step in phototransduction. Definitive estimates of the turnover number, k_{cat}, and of the K_m are crucial to quantifying the amplification contributed by the PDE. Published estimates for these kinetic parameters vary widely; moreover, light-dependent changes in the K_m of PDE have been reported. The experiments and analyses reported here account for most observed variations in apparent K_m, and they lead to definitive estimates of the intrinsic kinetic parameters in amphibian rods.

We first obtained a new and highly accurate estimate of the ratio of holo-PDE to rhodopsin in the amphibian ROS, 1:270. We then estimated the apparent kinetic parameters of light-activated PDE of suspensions of disrupted frog ROS whose structural integrity was systematically varied. In the most severely disrupted ROS preparation, we found K_m = 95 μM and k_{cat} = 4,400 cGMP·s^{-1}. In suspensions of disc-stack fragments of greater integrity, the apparent K_m increased to ~600 μM, though k_{cat} remained unchanged. In contrast, the K_m for cAMP was not shifted in the disc stack preparations.

A theoretical analysis shows that the elevated apparent K_m of suspensions of disc stacks can be explained as a consequence of diffusion with hydrolysis in the disc stack, which causes active PDEs nearer the center of the stack to be exposed to a lower concentration of cyclic GMP than PDEs at the disc stack rim. The analysis predicts our observation that the apparent K_m for cGMP is elevated with no accompanying decrease in k_{cat}. The analysis also predicts the lack of a K_m shift for cAMP and the previously reported light dependence of the apparent K_m for cGMP. We conclude that the intrinsic kinetic parameters of the PDE do not vary with light or structural integrity, and are those of the most severely disrupted disc stacks.

INTRODUCTION

The biochemical events underlying the activation phase of phototransduction in vertebrate retinal rods are now well understood (reviewed in Liebman, Parker, and

Address correspondence to Professor E. N. Pugh, Jr., Department of Psychology, University of Pennsylvania, Philadelphia, PA 19104-6196.

J. GEN. PHYSIOL. © The Rockefeller University Press · 0022-1295/94/06/1071/28 $2.00
Volume 103 June 1994 1071–1098

Dratz, 1987; Chabre and Deterre, 1989; McNaughton, 1990; Pugh and Lamb, 1990; Stryer, 1991; Pugh and Lamb, 1993). Photoisomerization causes rhodopsin to become an enzyme, catalytically activating the heterotrimeric GTP-binding protein (G_t, transducin) by catalyzing the exchange of bound GDP for GTP. The α-subunit of G_t complexed with GTP dissociates from the β,γ-subunits and activates phosphodiesterase (PDE) by relieving the inhibition imposed by the PDEγ subunits (Hurley and Stryer, 1982; Wensel and Stryer, 1986, 1990). This allows the catalytic α and β subunits of PDE to hydrolyze cGMP to GMP. The lowering of cytosolic cGMP in turn leads to the closing of cGMP-gated cation channels and hyperpolarization of the rod.

Quantitative understanding of the amplifying role played by the PDE in phototransduction requires accurate knowledge of its kinetic parameters. However, the kinetic parameters of PDE reported by different laboratories vary from 80 μM to > 1 mM for K_m, and from 300 to 2,000 cGMP s^{-1}/PDE for k_{cat} (Miki, Baraban, Keirns, Boyce, and Bitensky, 1975; Yee and Liebman, 1978; Robinson, Kawamura, Abramson, and Bownds, 1980; Sitaramayya, Harkness, Parkes, Gonzalez-Olivia, and Liebman, 1986; Kawamura and Murakami, 1988; Barkdoll, Pugh, and Sitaramayya, 1988; Dawis, Graeff, Heyman, Walseth, and Goldberg, 1988; Whalen, Bitensky, and Takemoto, 1990; reviewed by Gillespie, 1990, and by Pugh and Lamb, 1993). A light-induced increase in the apparent K_m of PDE has also been reported for gently disrupted but nonhomogenized rod outer segments (ROS) (Robinson et al., 1980; Kawamura and Murakami, 1986); these and other experiments suggest that the disc stack structure may systematically influence the apparent kinetic parameters of PDE.

The stack of discs enclosed by the plasma membrane of the ROS occupies ~50% of the intracellular space (Sidman, 1957; Korenbrot, Brown, and Cone, 1973). The discs are attached to the plasma membrane and to each other by microfilament bridges, and they maintain native spacing even in the absence of a plasma membrane (Cohen, 1971; Roof and Heuser, 1982). The disc stack is 60 μm in length in the intact frog ROS (~30 discs/μm or a total of 2,000 discs/rod), and can be broken by mechanical disruption into fragments of varying length. One purpose of this study was to replicate and extend the observation that systematic variations in the apparent kinetic parameters of PDE can be produced by experimental manipulations of the degree of structural integrity of the outer segment membranes (Kawamura and Murakami, 1986).

Diffusion of cGMP in the native disk stack plays an important role in phototransduction because excitation spreads longitudinally along the outer segment by cGMP diffusion. In intact rods, the disc stack structure severely retards the longitudinal diffusion of cGMP, perhaps by a factor of ≥30 (Lamb, McNaughton, and Yau, 1981; Lamb and Pugh, 1992; Olson and Pugh, 1993). Moreover, retardation of the radial diffusion of cGMP by binding may also occur in intact rods (Lamb and Pugh, 1992; Olson and Pugh, 1993). Diffusion of cGMP within the disc stack also can be a significant factor in biochemical experiments in which PDE activity is measured in preparations of disrupted outer segments that retain some degree of structural integrity. In such preparations, cGMP from the bulk solution must move into the stack by the relatively slow process of diffusion (as opposed to the rapid movement by convection that occurs in the bulk), and degradation of cGMP diffusing to PDEs that reside nearer the center of the stack must occur. Thus, a second purpose of this study has been to show that a theoretical model of "diffusion with hydrolysis" within disc

stacks can account for the observed variation in PDE kinetic parameters. We produce such a model and discuss its properties. In the discussion, we examine the consequences of our findings for the intrinsic kinetic properties of the PDE, and we estimate the amplification contributed by the PDE in intact amphibian rods.

MODEL OF PDE ACTIVITY IN THE DISC STACK

Description of the Disc Stack

Light micrographs of samples of the ROS preparations used for the measurement of PDE kinetic parameters are shown in Fig. 1 (×80). *A* contains intact ROS made accessible to small molecules and substrates by electropermeabilization (see Methods). These ROS are typically ~60 μm in length and 6 μm in diameter. In *B*

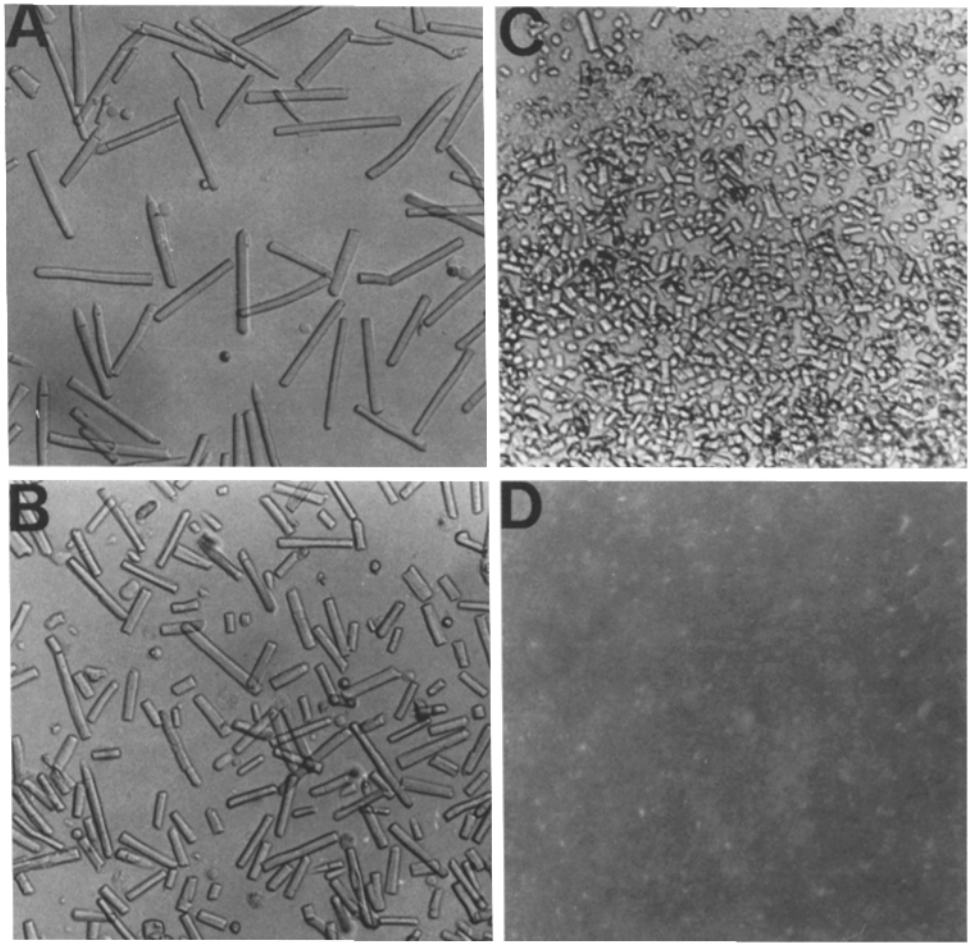

FIGURE 1. Light microscopy of four ROS preparations with increasing disruption. (*A*) Electropermeabilized ROS, (*B*) one-quarter to three-quarter length ROS segments, (*C*) one-fifth to one-tenth length ROS segments, and (*D*) completely disrupted ROS. All photomicrographs were taken at ×80 with conventional light microscopy.

one-quarter to three-quarter length ROS are shown, obtained by passing an intact ROS suspension 20 times through a 25-gauge needle attached to a 1-ml syringe. The shorter fragments in *C* one-fifth to one-tenth normal length were made with a Potter Elvehjem homogenizer by moving a loose-fitting Teflon pestle manually through the latter suspension 20 times. The completely disrupted ROS suspension shown in *D* was obtained by the same homogenizer with a tightly fitting motorized nylon pestle through the original ROS suspension 3–10 times. Fig. 2 presents scanning electron micrographs of the ROS preparations shown in Fig. 1, *B* and *D;* comparison of these microcraphs shows that the motorized pestle procedure produces completely disrupted fragments of discs. This latter preparation would be expected to present the shortest diffusional path for substrate access to the activated PDEs.

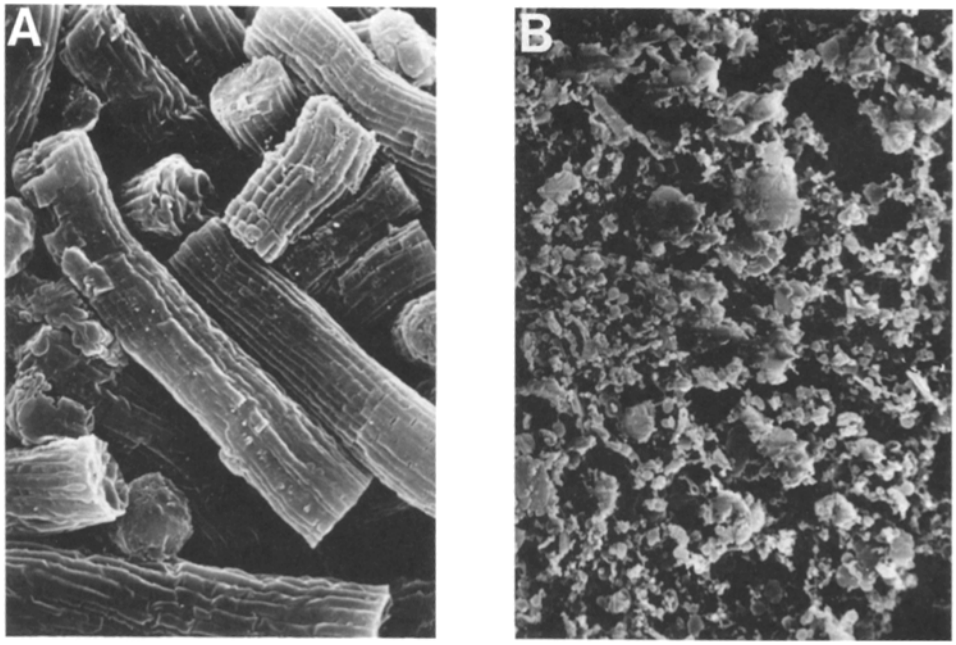

FIGURE 2. Scanning electron micrographs. Samples were prepared for SEM as outlined in Methods. (*A*) One-quarter to three-quarter length ROS segments (shown in Fig. 1 *B*) and (*B*) completely disrupted ROS (shown in Fig. 1 *D*). Both micrographs are at the same magnification; the width of the ROS fragments is ~6 μm.

Schematic of an ROS Fragment

Fig. 3 presents a schematic of a fragment of a frog ROS, highlighting the structural features important for our analysis of the PDE activity in a suspension of ROS fragments. The schematic in Fig. 3 is based on well-established physical descriptions of amphibian rods (reviewed in Rosenkrantz, 1977; Pugh and Lamb, 1993). Each rod fragment comprises a stack of discs, each with radius $a = 3$ μm; the interdiscal spacing is maintained by microfilament bridges, and it is similar to (but could differ from) that of the native rod, ~300 Å. Activated PDEs (*PDE**s) are attached to the

surface of the disc membranes. The left side of the panel presents an idealized disc stack with a completely disrupted plasma membrane; this stack is therefore fully patent to the bulk solution. The right side of the panel presents a disc stack with a partially intact plasma membrane and limited patency. The formal model of the disc stack we now develop will be based on the fully patent stack; a separate treatment will be provided for electropermeabilized ROS, whose cytoplasm is accessible to molecules in the bulk only through "pores" (see p. 1080 and Appendix).

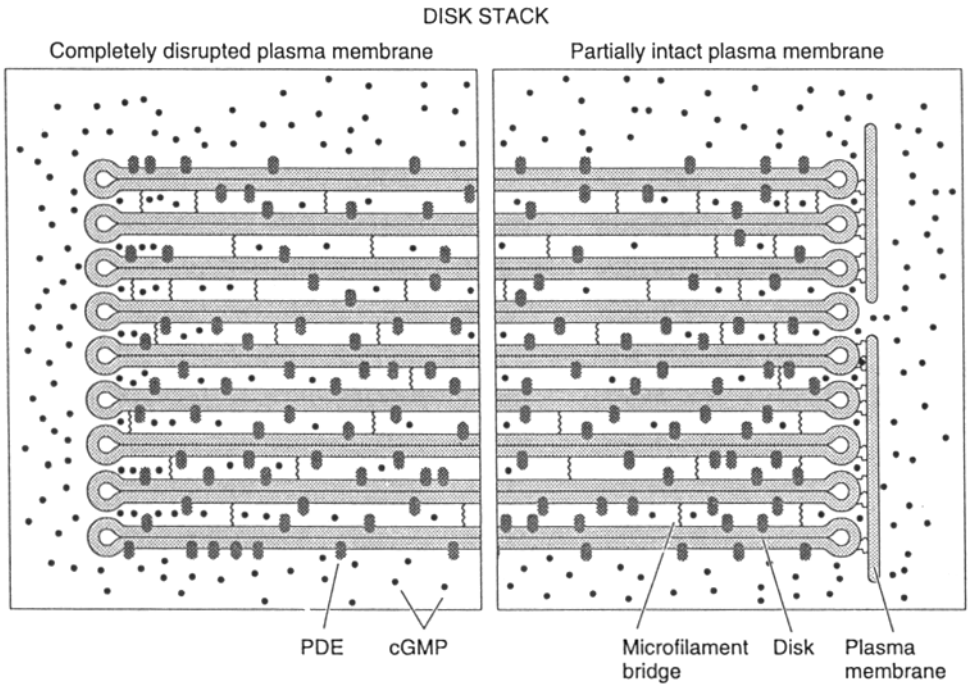

FIGURE 3. Schematic of ROS disc stack fragment. The organization of the disc stack fragment is maintained by microfilament bridges that span the discs. The dark, oblong structures attached to the disc faces represent *PDE**s, assumed uniformly distributed over the discs; the small filled circles represent molecules of cGMP, either in the surrounding bulk volume, or in the interdiscal spaces. The density of cGMP molecules in the interdiscal space is such as to illustrate qualitatively the effect of diffusion with hydrolysis in the stack. On the left side, the disc stack is shown fully patent to the bulk solution; the illustration on the right side has patches of plasma membrane attached to the disc stack so that the diffusional paths from the bulk to some *PDE**s exceed the disc radius.

Theoretical Description of the Disc Stack Preparation

The reaction system of a fully patent disc stack preparation consists of two aqueous compartments, the bulk volume of the cuvette, and the total interdiscal volume of the suspension of rod disc stacks. The reaction system is exposed to light (or $G_{t\alpha}$), so as to produce a fixed number of activated PDE molecules distributed uniformly over the discs. In the large, well-stirred bulk volume, cGMP molecules undergo fast, convec-

tive movements that maintain a uniform concentration, $[cGMP]_{bulk}$. In the narrow confines of the disc stack, cGMP can only move by the relatively slow process of diffusion. For a molecule of cGMP from the bulk to react with a *PDE** inside the stack, it must diffuse into the stack past other *PDE**s, and may be hydrolyzed in the process. Because of this "diffusion with hydrolysis," the concentration of cGMP at any position inside the disc stack is necessarily less than or equal to $[cGMP]_{bulk}$; in Fig. 3, we illustrate this effect schematically by showing a lower density of cGMP molecules near the center of the stack cross-section. Because [cGMP] near the disc stack center is always less than $[cGMP]_{bulk}$, it follows from that the total rate of cGMP hydrolysis exhibited by *PDE**s disposed in disc stacks will always be less than or equal to the rate exhibited by an equal number of *PDE**s on fully disrupted membranes.

To account quantitatively for the effect of the disc stacks on the apparent kinetic parameters of the PDE, we have developed a formal analysis of the diffusion with hydrolysis that governs the reaction of cGMP with *PDE**s in an open disc stack (Appendix). We now present the key features of the model, summarizing its behavior graphically (Fig. 4). We assume that the hydrolysis of cGMP by PDE obeys steady-state Michaelis-Menten kinetics locally; i.e.,

$$v = \frac{[E^*]k_{cat}[S]}{[S] + K_m}, \tag{1}$$

where v is the velocity of the reaction, $[E^*]$ is the enzyme concentration, $[S]$ is the concentration of substrate, k_{cat} is the turnover number, and K_m is the intrinsic or true Michaelis constant for the particular substrate. In saying that Eq. 1 applies "locally" to the disc stack preparation, we mean that $[E^*]$ must be interpreted as the concentration of *PDE**s with respect to some particular interdiscal volume within the stack, and likewise, that $[S\ ]$ is the concentration of substrate—say, of cGMP—in that same volume. In other words, since the reaction between *PDE**s and cGMP occurs almost exclusively within the disc stack, the actual concentrations of *PDE**s and cGMP determining the rate of hydrolysis of cGMP are those corresponding to the aqueous volume of fluid at some particular interdiscal location, and not the concentrations corresponding to the bulk or cuvette volume.

To express the local PDE activity in a form suitable for calculations, we consider now a single interdiscal space of radius a and height h. We then can rewrite Eq. 1 as

$$v(r) = [PDE^*]_{id}k_{cat}\frac{[cGMP]_r}{[cGMP]_r + K_m}, \tag{2}$$

where $v(r)$ is the PDE hydrolytic activity in molar units, $[PDE^*]_{id}$ is the molar concentration of active PDEs with respect to the interdiscal space, and $[cGMP]_r$ is the concentration of cGMP in a thin cylinder of infinitesimal width dr centered at radial position r, $r < a$. An important simplifying feature of the problem expressed in Eq. 2 is that *PDE**s are assumed to be uniformly distributed throughout the disc stack; thus $[PDE^*]_{id}$ is not a function of the radial coordinate r. It follows that we can write $[PDE^*]_{id} = PDE^*/(N_{Av}V_{id})$, where $V_{id} = h\pi a^2$ is the total aqueous volume of the interdiscal space, and *PDE** is the total number of fully active holo-PDEs attached to the disc surfaces bounding the interdiscal space, and N_{Av} is Avogadro's number.

In Eq. 2, K_m refers to the intrinsic Michaelis constant of the enzyme; i.e., to the Michaelis constant for PDE in a well-stirred experimental system where all *PDE**s have full access to the bulk. In Eq. 2, the steady-state concentration of cGMP in the disc stack is written as a function of r only (i.e., as $[cGMP]_r$); it follows from the cylindrical geometry of ROS that [cGMP] in the steady-state must be a radially symmetric function. Moreover, one can infer that because of hydrolysis, $[cGMP]_r$ always decreases steadily from the disc edge ($r = a$) to the center ($r = 0$) (Appendix).

Eq. 2 only gives the molar hydrolytic flux produced at some particular radial location in a single interdiscal space. The total molar flux v_{id} of an interdiscal space is obtained by integrating Eq. 2 over the interdiscal space, and dividing by the total interdiscal volume:

$$\begin{aligned} v_{id} &= \frac{1}{h\pi a^2}\int_0^a v(r)h2\pi r\mathrm{d}r \\ &= [PDE^*]_{id}k_{cat}\frac{1}{a^2}\int_0^a \frac{[cGMP]_r}{[cGMP]_r + K_m}\,2r\,\mathrm{d}r, \end{aligned} \tag{3}$$

where $h2\pi r\mathrm{d}r$ is the volume element of integration, and $h\pi a^2$ is the total volume of the interdiscal space. The condition linking the experimental variable $[cGMP]_{bulk}$ with the theory is that $[cGMP]_{r=a} = [cGMP]_{bulk}$.

No Effect of the Disc Stack on Estimates of k_{cat}

The particular case of Eq. 3 in which $[cGMP]_{bulk}$ is so high that $[cGMP]_r$ throughout the stack greatly exceeds K_m gives an important limiting condition. Thus, if for all r, $[cGMP]_r \gg K_m$, the integrand on the right-hand side of the second line of Eq. 3 becomes simply $2r\mathrm{d}r$, and the value of the integral is simply a^2: Eq. 3 then reduces to $v_{id} = (v_{id})_{max} = [PDE^*]_{id}k_{cat}$, the maximum PDE hydrolytic velocity of a single interdiscal space. This limiting case allows us to make an important prediction that we examine and verify experimentally: diffusion with hydrolysis in the disc stack per se cannot decrease the estimate of v_{max} (or k_{cat}): as long as all active enzymes are accessible by diffusion, the absolute v_{max} always can be achieved by raising the bulk substrate concentration sufficiently high. This prediction is more general than the radial model of the stack: even if the diffusional path is highly tortuous (see Fig. 3), the effect of diffusion with hydrolysis can be overcome, and the absolute v_{max} can always be achieved by raising the bulk substrate concentration sufficiently high. We emphasize that the prediction that the disc stack organization does not per se alter k_{cat} does not apply to electropermeabilized outer segments, which will be examined below in the Appendix.

Predicting Shifts in Apparent K_m

To compute the total molar hydrolytic flux v_{id} of an interdiscal space when [cGMP] varies across the stack as a function of r, one must specify the steady-state distribution $[cGMP]_r$ for the relevant disc and kinetic parameters, and then compute the integral in Eq. 3. For $[cGMP]_{bulk} \ll K_m$, $[cGMP]_r$ has a known analytical form that can be

readily integrated (Pugh and Lamb, 1993; Appendix). The steepness of decline of $[cGMP]_r$ from the disc stack edge is characterized by a "radial space constant," λ_r, which is expressible as a specific combination of disc stack parameters:

$$\lambda_r = \sqrt{\frac{D_r}{\beta}}. \tag{4}$$

In Eq. 4, D_r (in $\mu m^2 \cdot s^{-1}$) is the diffusion coefficient for cGMP diffusing radially in the disc stack; β is the rate constant (in s^{-1}) of PDE hydrolysis in the stack, and it is given by

$$\beta = [PDE^*]_{id} \frac{k_{cat}}{K_m} \frac{1}{BP}. \tag{5}$$

As before, $[PDE^*]_{id}$ is the molar concentration of fully activated PDEs with respect to the interdiscal volume, V_{id}. In Eq. 5, BP is the instantaneous buffering power of the cytosol for cGMP, which is expected to be 1–2 at normal physiological levels of cGMP (see Lamb and Pugh, 1992), but which is almost certainly equal to unity for the cGMP concentrations involved in the experiments reported here. The reciprocal of the rate constant, β^{-1}, represents the time constant for the complete hydrolysis of the cGMP in a disc stack when no cGMP is supplied exogenously. An important limiting case of Eq. 5 occurs when the total complement of PDE is activated; in this case, we identify the rate constant as β_{max}. (For further discussion of Eqs. 4 and 5, see Pugh and Lamb, 1993.)

Fig. 4 shows distributions of cGMP, cAMP, and corresponding PDE activities derived with the model, subject to the condition $[S]_{bulk} \ll K_m$. The unbroken curves give the predicted steady-state distribution of nucleotide across the disc stack; the coarsely dashed curves give $rv(r)/av(a)$, the radially weighted PDE activity distribution over r predicted by Eq. 2 (see caption and Appendix). The presentation chosen for the PDE activity curves in Fig. 4 is such that the fractional reduction in observed PDE activity produced by the effect of the disc stack can be seen as the area under the coarsely dashed curve, relative to the area under the positive diagonal (which represents the weighted PDE activity for a uniform substrate distribution across the stack; see caption). The particular sets of kinetic parameters chosen for these curves are those that provide an account of key features of the data presented below (Fig. 5; Table I).

For $[cGMP]_{bulk} \ll K_m$, the diminished rate of hydrolysis of PDE^*s disposed in a disc stack (relative to the rate that would be produced by the same number of PDE^*s disposed on fully disrupted membranes) can be compensated for by raising $[cGMP]_{bulk}$. Since, as we have noted above, an essential feature of diffusion with hydrolysis is that the absolute v_{max} can be attained at sufficiently high $[cGMP]_{bulk}$, it follows that the overall effect of the disc stack is to shift the apparent K_m to a higher value, K'_m (Appendix). We will refer to the ratio $\rho = K'_m/K_m$ as the "K_m shift." From Eq. 3, it can be shown that ρ obeys the relation

$$\rho = \frac{K'_m}{K_m} = \frac{[cGMP]_{r=a}}{\frac{1}{a^2}\int_0^a [cGMP]_r \, 2r \, dr}, \tag{6}$$

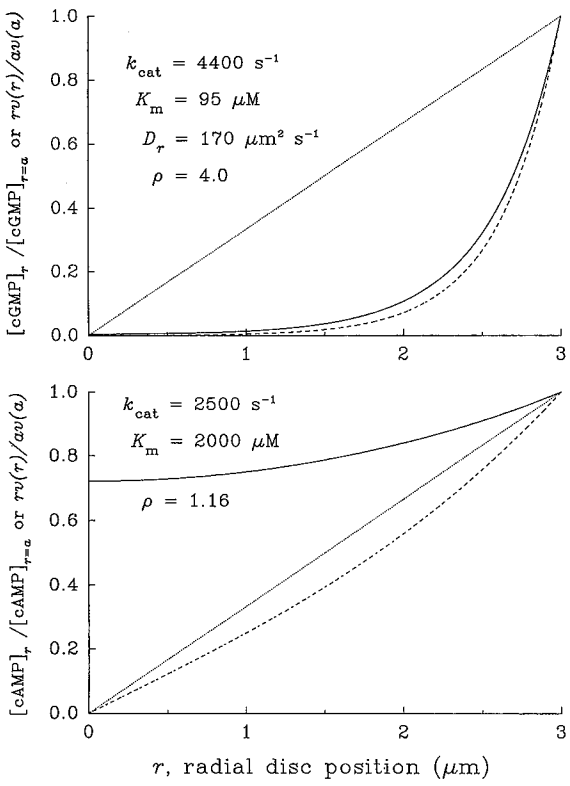

FIGURE 4. Predictions of the model of the disc stack. Calculations of the diffusion with hydrolysis open disc stack model are shown in *A* for PDE hydrolysis of cGMP, and in *B* for cAMP. The common abscissa is the radial position r within the disc stack ranging from $r = 0$ (the center of the stack) to $r = a$, the radius of the frog rod; a is fixed at 3 μm.

The unbroken line in each panel gives the predicted distribution of nucleotide across the disc stack, computed for the condition $[\text{nucleotide}]_{bulk} \ll K_m$, where K_m is the intrinsic Michaelis constant of the PDE for the nucleotide; the nucleotide distribution is normalized to its value at $r = a$, the disc edge, where it is assumed equal to the bulk concentration. (The distribution $[\text{cGMP}]_r$ of nucleotide was computed with Eq. 13, the Bessel function of order 0, as described in the Appendix.) The coarsely dashed line in each panel gives the radially weighted PDE activity across the disc stack, normalized to the PDE activity at the disc stack edge, as described by Eq. 2 of the text, for the nucleotide distribution shown by the unbroken line. For the condition $[\text{nucleotide}]_{bulk} \ll K_m$, the weighted PDE activity, $rv(r)/av(a)$, is equal to $r[\text{nucleotide}]_r/a[\text{nucleotide}]_{r=a}$.

In the two examples shown here, all the PDE of the outer segment was assumed to be fully activated; this yields $[PDE^*]_{id}$ = 22 μM, assuming $[Rh]$ = 0.006 M with respect the interdiscal space, and Rh/PDE = 270:1. The specific kinetic parameters determining $[\text{nucleotide}]_r$ in each case are shown on the plot: k_{cat}, the turnover number of the holo-enzyme; K_m, the intrinsic Michaelis constant for the nucleotide; D_r, the assumed radial diffusion coefficient for the nucleotide in the interdiscal space (assumed to be the same for both nucleotides). The predicted shift in apparent K_m in each case can be seen visually as the ratio of the area under the weighted PDE activity distribution, relative to the area under the positive diagonal (*dotted curve*), as explained in the text (see Eq. 6); the positive diagonal gives the predicted PDE activity curve in the case where there would be no variation across the disc stack; i.e., where $[\text{nucleotide}]_r = [\text{nucleotide}]_{bulk}$ for all r. Thus, with the radial diffusion coefficient D_r = 170 μm^2·s^{-1}, a K_m shift of ρ = 4.0 for cGMP is predicted, as observed for the small fragment preparation (Table I); with the same value of D_r, the K_m shift predicted for cAMP is ρ = 1.16; i.e. only a 16% increase.

where as before, for the open disc stack, we have $[\text{cGMP}]_{r=a} = [\text{cGMP}]_{bulk}$. Note that $\rho \geq 1$, since $[\text{cGMP}]_r \leq [\text{cGMP}]_{r=a}$.

From inspection of Eqs. 4–6, one can see that factors diminishing λ_r will necessarily increase the apparent K_m (see Fig. 4). This follows because the smaller the value of λ_r,

the more steeply $[cGMP]_r$ declines from disc edge to center, and the greater the reduction in overall PDE activity. Thus, the smaller the value of λ_r, the higher $[cGMP]_{bulk}$ must be raised to achieve a given level of PDE activity. In summary, according to Eq. 4, decreasing D_r will diminish λ_r and increase the apparent K_m. Likewise, according to Eqs. 4 and 5, increasing $[PDE^*]$ and k_{cat} will increase the apparent K_m.

With the insight that diffusion with hydrolysis in the disc stack acts to shift the apparent K_m to a higher value than the intrinsic K_m, we can write a useful phenomenological relation for v_{id} when $[cGMP]_{bulk} \ll K_m$:

$$v_{id} = \frac{[PDE^*]_{id} k_{cat} [cGMP]_{bulk}}{K'_m}. \tag{7}$$

Eq. 7 links the apparent PDE kinetic parameter K'_m with the experimental variable, $[cGMP]_{bulk}$.

Relation between Hydrolysis Predicted to Occur in the Interdiscal Space and That Measured in the Reaction Cuvette

The data of our experiments consist of the steady-state hydrolytic velocities of suspensions of disc membranes, measured in the bulk. To compare theory with data, we must compute the total molar hydrolytic flux produced by a suspension of disc stacks for a given bulk concentration of cGMP. The general relationship between the hydrolysis rate predicted for the single interdiscal space and that measured in the reaction cuvette is the following:

$$\begin{aligned} v_{cuvette} &= v_{id} \frac{[PDE^*]_{cuvette}}{[PDE^*]_{id}} \\ &= v_{id} \frac{[Rh]_{cuvette}}{[Rh]_{id}}, \end{aligned} \tag{8}$$

where $v_{cuvette}$ refers to the experimentally measured PDE hydrolytic velocity (in $M \cdot s^{-1}$). This relation holds for any $[cGMP]_{bulk}$, and when combined with Eqs. 3–7, allows comparison of theory and data. Specifically, the second line of Eq. 8 follows from the first by virtue of the invariant ratio of Rh/PDE on the disc membranes, a ratio that must also be equal to the concentration ratios $[Rh]_{id}/[PDE]_{id}$ and $[Rh]_{cuvette}/[PDE]_{cuvette}$. In sum, the second line of Eq. 8, when combined with the formula for v_{id} in Eq. 3 and the ratio of Rh/PDE on the disc membranes (Results), predicts $v_{cuvette}$.

Extension to Electropermeabilized ROS

As we have seen, the "diffusion with hydrolysis" model of the open disc stack predicts a upward shift in the apparent K_m of the open disc stack preparations. The model also predicts that the k_{cat} of a disc stack preparation should not be altered from that value derived from the fully disrupted membranes. This follows, since raising $[cGMP]_{bulk}$ sufficiently high can raise $[cGMP]_r$, even at the center of the stack well above the K_m. A characteristic feature of the measured PDE activity of the electropermeabilized ROS preparation, however, is that the apparent k_{cat} is diminished (Fig. 5;

Table I), a fact inconsistent with mere diffusion with hydrolysis. Moreover, the electropermeabilized ROS also shows a shift of the apparent K_m well beyond the apparent value obtained from the ROS fragment preparations. These two striking features of the electropermeabilized ROS preparation can be accounted for by an extension of the model in which the outer segment membrane has a limited permeability to cGMP (Appendix). The general steady-state assumption applied to the electropermeabilized ROS requires that the measured hydrolytic flux corresponds to the net inward flux of cGMP through the permeabilized ROS membrane. This assumption and the use of Fick's Law are the basis of the extended model (Appendix).

The diminished apparent k_{cat} of the electropermeabilized preparation leads to an estimate for the maximum possible flux of cGMP through the permeabilized membrane; the shift in apparent K_m greater than the value in the open stack preparation leads to an estimate of the permeability constant for cGMP.

We now turn to the experimental results, and show how the data and model yield estimates of k_{cat} and the intrinsic K_m, and also lead to estimates of D_r, the radial diffusion coefficient of cGMP in the disc stack, and of the permeability constant for cGMP of the electropermeabilized ROS membrane.

METHODS

Materials

[8,5′-^{3}H]cGMP and [2,8-^{3}H]cAMP were purchased from Du Pont-New England Nuclear (Boston, MA), Percoll and Sephadex A25 from Pharmacia LKB Biotechnology Inc. (Piscataway, NJ), potassium isethionate from Kodak Corp. (Rochester, NY), and Ecoscint from National Diagnostics, Inc., (Atlanta, GA). All other chemicals were obtained from Sigma Immunochemicals (St. Louis, MO).

Solutions

The Ringer's solution used to isolate ROS contained: 105 mM NaCl, 2 mM KCl, 2 mM $MgCl_2$, 1 mM $CaCl_2$, and 10 mM HEPES, pH 7.5. The pseudointracellular medium used in all experiments contained 95 mM potassium isethionate, 15 mM sodium isethionate, 5 mM $MgCl_2$, 2 mM dithiothreitol, 10 μM leupeptin, 100 kallikrein U/ml aprotinin, and 10 mM HEPES, pH 7.8. All the solutions had a final osmolarity of 232–238 mosM.

Preparation of ROS

Live bullfrogs (*Rana catesbiana* or *Rana grylio*) were purchased from commercial sources and maintained on a 12-h light/12-h dark cycle $\geq$2 wk before use (Woodruff and Bownds, 1979). All manipulations were done in the dark under infrared illumination. Animals were killed by decapitation, the retinas were removed and placed into Ringer's solution containing 5% Percoll, and ROS were purified on a Percoll gradient as described previously (Biernbaum and Bownds, 1985). Intact ROS were washed free of Percoll in pseudointracellular medium and kept on ice before experiments. Rhodopsin concentration was determined spectrophotometrically according to Bownds, Gordon-Walker, Gaide-Huguenin, and Robinson (1971).

Electropermeabilized ROS (Gray-Keller, Biernbaum, and Bownds, 1990) were obtained by placing an intact ROS suspension in a 120-μl cell chamber between two stainless steel electrodes 4 mm apart. A gene pulser (Bio-Rad Laboratories, Richmond, CA) was used to generate 3–6 pulses at 2,000 V/cm with a time constant of ~4 ms. This preparation was found to optimize substrate accessibility to ROS internal enzymes yet retain most soluble proteins. A medium molecular weight polysaccharide [15 mM dextran (M_r = 6,000)] was added to the pseudointracellular medium to balance the colloid osmotic pressure caused by internal proteins. Scanning electron micrographs were made using a scanning electron microscope (S-570; Hitachi Instruments, Inc., San Jose, CA). Samples were fixed in 5% glutaraldehyde and dehydrated in a series of alcohol steps.

Purified $G_{t\alpha}$-GTPγS Preparation

Purified $G_{t\alpha}$-GTPγS was prepared from toad ROS as described earlier (Arshavsky, Dumke, and Bownds, 1992). A ROS suspension was bleached to achieve tight binding of G_t to rhodopsin, and washed in 5 mM Tris-HCl, pH 8.0, 0.5 mM EDTA, and 1 mM dithiothreitol to extract PDE. To obtain the $G_{t\alpha}$-GTPγS complex, after PDE extraction, the membranes were washed twice with 100 μM GTPγS in the pseudointracellular medium. After concentrating with a Centricon-30 cartridge, the extract was purified in the same medium on a Superose-12 column (Pharmacia LKB Biotechnology Inc.). The purity was determined by SDS-electrophoresis to be >98%. Protein concentration was measured by a modification of the Bradford assay (Bradford, 1976; Chumakov, Rozanov, and Agol, 1982) using bovine serum albumin as a standard.

Quantitation of PDE/Rhodopsin Ratio

The amount of PDE in amphibian ROS was determined by scanning gel electrophorograms containing whole ROS and purified PDE as a standard. PDE was purified as described earlier (Arshavsky and Bownds, 1992, Arshavsky et al., 1992). PDE concentration was determined by amino acid analysis of the purified protein. A series of whole ROS concentrations and PDE standards were loaded on the same gel. The gels were stained by Coomassie G-250 and the densities of PDE bands were analyzed using a Fotodyne Foto/analyst® system and Collage® software (Fotodyne, New Berlin, WI).

PDE Activity Measurements

PDE activity was determined by a radioisotope assay (Hurley and Stryer, 1982; reviewed in Kincaid and Manganiello, 1988). The reaction was started by mixing 20 μl of ROS suspension with 20 μl of radiolabeled cyclic nucleotide, cGMP, or cAMP, (with GTP or GTPγS, if necessary) in a 1.5-ml Eppendorf tube while vortexing gently; this vortexing did not produce any changes in the size of the rod fragments. (For the electropermeabilized ROS, gentle manual stirring, not vortexing, was used to mix reagents into the suspension.) The reactions were stopped with 100 μl of 0.1 M HCl. The samples were then neutralized with 0.1 M Tris and treated for ~20 min with 50 μl of *Ophiophagus hannah* snake venom (1 mg/ml) to convert [^{3}H]GMP or [^{3}H]AMP formed during the cGMP hydrolysis into [^{3}H]guanosine or [^{3}H]adenosine. [^{3}H]guanosine or [^{3}H]adenosine, was separated from cGMP or cAMP on minicolumns with 0.7 ml of DEAE Sephadex A-25. The columns were washed twice with 0.8 ml H_2O. The eluate was mixed with 10 ml of Ecoscint and counted on a liquid scintillation counter (2000CA; Packard Instruments, Meriden, CT).

Estimation of Kinetic Parameters

Michaelis saturation functions (Eq. 9) were fit to initial velocity vs substrate concentration data in linear/linear format with the Marquardt-Levenberg least squares algorithm available in

SigmaPlot®. The fitting procedure provided estimates of v_{max} and K_m from each experiment (as shown in Fig. 5); the coefficients of variation of the parameter estimates obtained from fitting individual data sets were in every case $<10\%$. Similarly, the Hill equation was fitted to membrane concentration vs PDE activity data to estimate the cooperativity (Fig. 6).

RESULTS

Determination of Rhodopsin/PDE Ratio

From five determinations, the rhodopsin/PDE ratio in the frog ROS was estimated as 270 ± 35 (mean ± SEM); the individual estimates ranged from 240:1 to 320:1. This revises an earlier, more approximate estimate (Hamm and Bownds, 1986). Hereafter, we report PDE-specific activity, calculated on the basis of $[Rh]_{cuvette}$, the measured rhodopsin content of the sample, and the Rh/PDE ratio 270:1 (cf Eq. 8). For future reference, assuming $[Rh]_{id}$, the concentration of rhodopsin referred to the native interdiscal space to be 6 mM, we obtain $[PDE^*]_{id}$ = 22 μM, assuming all the PDEs are activated.

Measurement of PDE Activity in ROS Suspensions

Fig. 5 shows PDE hydrolytic rates plotted as function of bulk [cGMP] for individual experiments with the four preparations illustrated in Fig. 1. In each case, a Michaelis saturation fucntion has been fit to the data:

$$\frac{v}{[PDE^*]} = k_{cat}\frac{[\text{cGMP}]}{[\text{cGMP}] + K_m}, \tag{9}$$

where $v = v_{cuvette}$, and we suppress the subscript; likewise, the concentrations $[PDE^*]$ and [cGMP] are those with respect to the bulk volume of the reaction cuvette, and we suppress the subscripts. Thus, $v/[PDE^*]$ is the apparent specific activity. (In writing Eq. 9, and in referring to its application to individual data sets, we use the symbols k_{cat} and K_m to refer to apparent kinetic parameters; the adjectives "apparent" and "intrinsic" will be used as needed for clarity. The symbol K'_m will be used only when needed for mathematical clarity.) The left-most data set (Fig. 5, *filled circles*) was obtained from the most severely disrupted membranes; the best-fitting Michaelis function for this set of data yielded the parameter estimates k_{cat} = 4,240 s^{-1}, and K_m = 94 μM. The middle two data sets (Fig. 5, *open and closed triangles*) were obtained with ROS fragments of one fifth to one tenth and one quarter to three quarters the length of the outer segment, respectively. These data are well characterized by Eq. 9 with values of k_{cat}—4,510 s^{-1} and 4,300 s^{-1}, respectively—nearly identical to that (4,240 s^{-1}) for the curve fit to the most severely disrupted ROS membranes. However, the value of the apparent K_ms for the two curves are shifted upward to 325 and 510 μM, respectively. Finally, the rightmost data set (Fig. 5, *open squares*) was obtained from a suspension of electropermeabilized ROS; it is characterized by the apparent kinetic parameters k_{cat} = 1,970 s^{-1} and K_m = 3,000 μM.

Table I provides a summary of the analyses of a series of such experiments on the four preparations, with both cGMP and cAMP as substrates for the reaction. There were no statistically reliable differences in the estimates of k_{cat} for cGMP among the first three preparations—completely disrupted ROS, small ROS fragments, and large ROS fragments—as confirmed by a one-way analysis of variance [$F(2,7) = 2.2$,

$P > 0.10$]. In contrast, the estimates of the apparent K_m varied highly systematically in the manner illustrated in Fig. 5.

The fact that the values of the apparent k_{cat}s of the two disc stack fragment preparations are statistically the same as that of the fully disrupted membranes is consistent with the theoretical analysis of the disc stack preparation: i.e., at suffi-

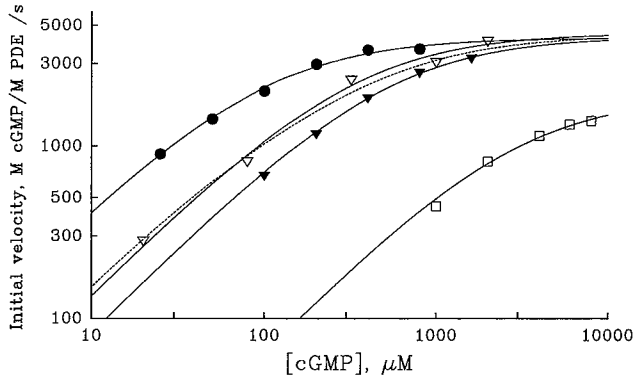

FIGURE 5. PDE activity in the four ROS preparations: dependence of apparent K_m on the size of the rod fragments. The abscissa indicates the logarithm of the concentration of cGMP substrate in the reaction cuvette, $[cGMP]_{bulk}$; the ordinate shows the logarithm of the specific velocity or activity. Initial rates were determined for at least five different substrate concentrations. Data were fit with Michaelis saturation functions, Eq. 9 (see Methods), to obtain the apparent kinetic parameters K_m and v_{max}, where v_{max} is the initial velocity of the reaction in M cGMP hydrolyzed s^{-1} for a given preparation and nucleotide concentration. Specific activities (M nucleotide hydrolyzed per M PDE s^{-1}) were then calculated with the determined *Rh/PDE* ratio of 270:1; k_{cat} was estimated as the saturated value of the specific activity.

The leftmost data set (*filled circles*) gives data from the most fully disrupted outer segments. The open and closed triangles are the data from the small and large ROS disc stack fragment preparations respectively. The rightmost data set (*open squares*) are data from an electropermeabilized ROS preparation. The unbroken curves are the Michaelis functions (Eq. 9) best fitting each data set; the apparent kinetic parameters k_{cat} and K_m characterizing these curves are given in the text. (Though plotted in double-log format, the data were fit with Michaelis functions in double-linear format.) The apparent K_ms of the small and large disc stacks are 3.5 and 5.4 times greater, respectively, than that of the completely disrupted preparation, whereas the apparent K_m of the electropermeabilized ROS is shifted > 30-fold (see text). The dashed curve is a curve best fitting the small-fragment data, based on the hypothesis that the small fragment preparation is a mixture of 20% fully disrupted disc membranes, and 80% patent disc stacks; it was generated as the sum of two weighted Michaelis functions with K_ms of the large-fragment (510 μM) and the fully disrupted (94 μM) ROS membranes, respectively. Each set of data is taken from one of three experiments that yielded similar results. Table I presents summary statistics of the parameters estimated from the entire set of experiments.

ciently high values of $[cGMP]_{bulk}$, the same number of *PDE**s per rhodopsin is active in each preparation and saturated with substrate. Therefore, we can take the overall mean of the estimates of k_{cat} from these three preparations, 4,400 s^{-1}, as our best estimate for the intrinsic k_{cat} of the fully light-activated holo-PDE of amphibian ROS.

In Fig. 5, the apparent K_m of the smaller disc stack fragment (one-fifth to one-tenth) preparation is shifted upward by a factor of 3.5 from that of the most fully disrupted membranes; the average K_m-shift of the small disc fragment preparation obtained from the complete data of Table I is fourfold. These data are consistent with the qualitative conclusion that the intrinsic K_m is that of the most disrupted membrane preparation, 95 μM, and that the upward shift in apparent K_m of the small fragment preparation is caused by diffusion with hydrolysis of substrate in the stacks. This conclusion is supported quantitatively by the theoretical results presented in Fig. 4 *A* (see Eq. 6); there, it is illustrated that a fourfold K_m-shift from 95 to 380 μM is predicted by the theoretical model, providing D_r, the radial diffusion coefficient of cGMP, is 170 $\mu m^2 \cdot s^{-1}$.

TABLE I

Kinetic Parameters of PDE Estimated from Different ROS Preparations

	k_{cat}	K_m	ρ
A cGMP as substrate	s^{-1}	*μM*	
1. Completely disrupted ROS	4,170 ± 370	95 ± 40	1.0
2. One-fifth to one-tenth ROS fragments	4,000 ± 510	380 ± 54	4.0
3. One-quarter to three-quarter ROS fragments	5,070 ± 1,080	610 ± 140	6.4
4. Electropermeabilized ROS	2,040 ± 300	3,150 ± 350	33
B cAMP as substrate			
1. Completely disrupted ROS	2,500 ± 120	2,040 ± 250	1.0
2. One-quarter to three-quarter ROS fragments	2,340 ± 260	1,980 ± 110	1.0

K_m and K_{cat} values were obtained from fitting Michaelis saturation functions (Eq. 9) to data of the four preparations, as illustrated in Fig. 5, and explained in Methods. The empirical estimates of ρ, the K_m shift, were obtained as the ratio of the K_ms for the fragment preparations to those of the completely disrupted ROS for each substrate. PDE-specific activities (M cGMP hydrolyzed/M PDE /s) were calculated with the *Rh/PDE* ratio of 270:1 (see Eq. 8). Each entry in the table is the mean ± SD obtained from three complete experiments such as shown in Fig. 5.

The value of the apparent K_m of the preparation consisting of larger (one-quarter to three-quarter) ROS fragments is shifted higher, on average by a factor of 1.6 (Table I) above the value for the small fragment preparation. This result is not consistent with the hypothesis that the small and large fragment preparations are both fully open to the bulk solution, because the hypothesis predicts that these two preparations should have the same apparent K_m. One possible resolution is sketched in Fig. 3. The right-hand side of the schematic shows patches of plasma membrane still attached to the disc stack; such patches seem likely to be present (see Figs. 1, *B* and *C*, and 2 *A*). Patches of membrane necessarily increase the distance over which cGMP must diffuse from the bulk solution to reach *PDE**s, and increased diffusional path length will cause the concentration of cGMP in the interior of the disc stack to be overestimated by the radial model (for any given set of model parameters). To

account quantitatively for the further K_m shift of the one-quarter to three-quarter fragment preparation within the framework of the fully open disc stack model, one would have to postulate a lower value of D_r; for example, if the intrinsic kinetic parameters are k_{cat} = 4,400 s^{-1}, K_m = 95 μM, one requires D_r = 80 $\mu m^2 \cdot s^{-1}$ to produce a 6.4-fold K_m shift to 610 μM. We think it is unlikely that the radial diffusion coefficient could be diminished so far below its free aqueous value of ~500 $\mu m^2 \cdot s^{-1}$, and so we propose as one explanation that the additional shift is caused by a lengthened diffusional path (Fig. 3). However, we have not attempted to make a formal model that would incorporate a lengthened diffusional path.

An alternative explanation for the differences in the apparent K_ms of the small- and large-fragment preparations is that the small-fragment preparation contains more isolated discs or disc fragments. This might be expected, since the small fragment preparation was subjected to greater shearing forces. A downward shift of apparent K_m from 600 to 400 μM would require that ~20% of the disc membranes in the small fragment preparation are totally disrupted; the dashed line in Fig. 5 illustrates a saturation function derived from this hypothesis (see figure caption). Although the hypothesis of such an admixture of fully disrupted disc membrane material cannot be ruled out, it implicitly requires that the large fragment preparation be fully patent at its edges; and as noted above, predicting its 6.4-fold K_m-shift above that the completely disrupted membranes requires D_r = 80 $\mu m^2 \cdot s^{-1}$, which we believe to be unlikely.

The data in Table I *B* show that the apparent K_m for cAMP is not affected by the structural integrity of the disc fragments. In combination with the strong effect of structural integrity on the apparent K_m for cGMP, the lack of effect on the K_m for cAMP supports the interpretation that the primary effect of ROS structural integrity is to increase the diffusional path of substrate from the bulk to *PDE**s near the center of the disc stacks. In Fig. 4 *B*, we show that this interpretation is also in rough quantitative agreement with the prediction of the open disc stack model. There, is it shown that if the intrinsic kinetic parameters for cAMP are taken to be those of the fully disrupted ROS, k_{cat} = 2,500 s^{-1}, K_m = 2,000 μM (Table I *B*), and if D_r = 170 $\mu m^2 \cdot s^{-1}$ for cAMP, there should be a 16% upward shift in the apparent K_m for cAMP of the small fragment preparation. One way to explain the observed result (that there is no shift of the apparent K_m of the large fragment preparation) is to hypothesize that cAMP can diffuse in the ROS faster than can cGMP: for example, the K_m shift predicted is <10%, the error of measurement, if D_r = 300 $\mu m^2 \cdot s^{-1}$ for cAMP. An alternative explanation is that the apparent K_m for cAMP has been underestimated: a shift of <10% is predicted for K_m = 2,800 μM and D_r = 170 $\mu m^2 \cdot s^{-1}$. Combinations of these hypotheses, such as K_m = 2,500 μM and D_r = 250 $\mu m^2 \cdot s^{-1}$, also predict a K_m shift that would be less than the error of measurement.

As shown in Fig. 5 and Table I, two features distinguish the apparent kinetics of PDE in the electropermeabilized ROS preparation from the kinetics of the other preparations: (*a*) a diminished value of the apparent k_{cat} and (*b*) a further upward shift (roughly eightfold) in K_m beyond that of the small fragment preparation. Caution is called for in interpreting the numerical estimate of apparent k_{cat} because the range of cGMP concentrations used may not have been high enough for an

accurate determination of v_{max}. Nonetheless, the velocity data show clear evidence of approaching saturation (see two highest open squares in Fig. 5), and the qualitative effect of a diminished apparent k_{cat} seems unassailable.

Explanation of a diminished apparent k_{cat} requires a generalization of the "diffusion with hydrolysis" model that incorporates a maximal or absolute upper limit to the inward cGMP flux, and a finite permeability of the permeabilized membrane for cGMP (Appendix). The upper limit to the inward flux can be computed from the data of Fig. 5 and Table I, based on the assumption that at steady state the total inward flux of cGMP through the electropermeabilized membrane must equal the total hydrolytic flux. The maximum hydrolytic flux is found to be $\sim 3 \times 10^{10}$ molecules·s^{-1} per ROS, which for a 60-μm ROS having a surface area of ~ 600 μm^2, gives a maximum flux density of 5×10^7 molecules·μm^{-2}·s^{-1} through the electropermeabilized membrane.

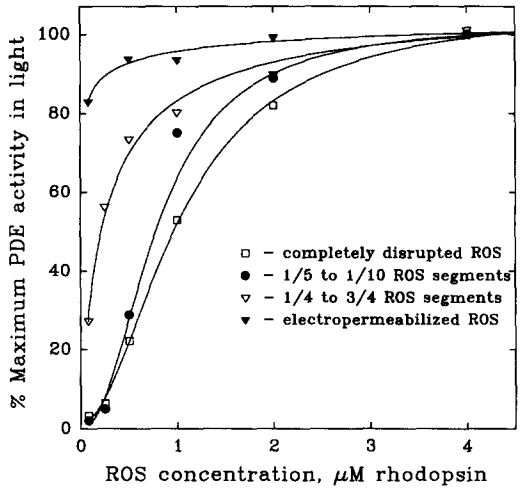

FIGURE 6. PDE activity is diminished by dilution of the ROS fragment suspension. PDE activities were measured using saturating light, GTP, and cGMP. Activities were determined at the indicated rhodopsin concentrations in the four different ROS suspensions shown in Fig. 1: (*open squares*) completely disrupted ROS, (*closed circles*) one-fifth to one-tenth ROS segments, (*open triangles*) one-quarter to three-quarter ROS segments, and (*closed triangles*) electropermeabilized ROS. Curves were fit with the Hill equation with a Hill coefficient equal to 1 for electropermeabilized ROS, 2.1 for ¼–¾ segments, 2.7 for one-fifth to one-tenth segments, and 2.1 for completely disrupted ROS. The data are from one of three experiments that yielded similar results.

Loss of PDE Activity in Diluted ROS Suspensions

A problem relevant to determining the PDE hydrolytic velocities reported in Fig. 5 and Table I encountered in these experiments deserves description. As disrupted ROS suspensions are diluted below concentrations of 4.0 μM rhodopsin, a progressive loss of the maximal activity obtainable was observed. Only in electropermeabilized ROS suspensions was PDE activation retained at low bulk rhodopsin concentrations. This result is illustrated in Fig. 6, in which PDE activity is measured in the four ROS preparations described in Fig. 1 as each suspension is progressively diluted from 4.0 to 0.08 μM rhodopsin. The decay of activity that accompanies dilution shows an apparent cooperativity with respect to ROS concentration.

In Fig. 7, we show data that argue that the loss of PDE activity on dilution most likely results from dissociation of membrane bound $G_{t\alpha}$. When exogenous purified $G_{t\alpha}$-GTPγS is added to diluted ROS, PDE activity is largely restored. Addition of 0.4 μM $G_{t\alpha}$-GTPγS to completely disrupted 4 μM ROS (thereby doubling the concentration of G_t, for there is 1 G_t for every 10 rhodopsins in the ROS) has little effect, indicating that the endogenous pool of G_t is sufficient to fully activate PDE. The lower PDE activity (10%) in completely disrupted 0.25 μM ROS, however, is not saturated by the endogenous pool of G_t. The addition of 0.8 μM $G_{t\alpha}$-GTPγS permits almost complete recovery of maximum velocity. A practical consequence of these observations is that disrupted ROS suspensions must always be kept at concentrations containing ≥4 μM rhodopsin to avoid a dilution artifact in determining v_{max}.

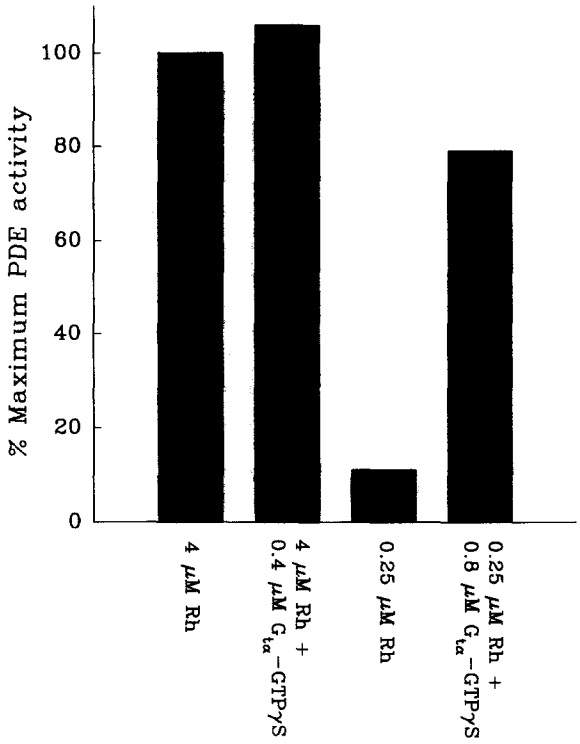

FIGURE 7. Loss of PDE activation caused by dilution is reversed by addition of excess amounts of PDE activator, $G_{t\alpha}$. Using the conditions of Fig. 6, PDE activities were measured in completely disrupted ROS preparations at two different rhodopsin concentrations, 4 μM and 0.25 μM. Purified $G_{t\alpha}$-GTPγS was added in the indicated amounts. The data are taken from one of three similar experiments. PDE activity was determined, and was then normalized as the percent of the specific activity observed in 4 μM rhodopsin without added $G_{t\alpha}$.

DISCUSSION

Intrinsic Kinetic Parameters of the Light-activated Frog Rod Phosphodiesterase

We found that the maximum hydrolytic velocities of the PDE of the three ROS disc fragment preparations were statistically the same, a result expected if the sole effect of the degree of structural integrity of the disc stacks of these preparations is to alter the diffusional path that the substrate must take to reach active *PDE**s. Based on this result and our new estimate of the total number of holo-PDEs per ROS, we conclude that the intrinsic turnover number of the light-activated amphibian rod holo-enzyme

is 4,400 s^{-1}. Based on the general agreement of the diffusion with hydrolysis model and the pattern of apparent K_ms of the disc fragment preparations, we also conclude that the intrinsic K_m of the PDE is 95 μM. This latter estimate is consistent with a previous report of the K_m obtained from vigorously disrupted and fully light-activated frog ROS membranes (Yee and Liebman, 1978).

It has been established that the holo-PDE consists of two homologous but distinct catalytic subunits, PDE_α and PDE_β, each associated with a γ subunit whose "relief" serves to activate the catalytic subunit (reviewed in Pugh and Lamb, 1993). The results reported here make no effort to distinguish possible differences in the intrinsic parameters of the two catalytic subunits. Treating the two catalytic subunits as having indistinguishable kinetic parameters allows us to estimate $k_{cat}/K_m \sim 2.3 \times 10^7\ M^{-1}\cdot s^{-1}$ for each subunit, showing that the hydrolytic reaction occurs near the diffusion limit. We recently have found the activity of PDE in fully dark-adapted ROS to be lower than the detection limits of our assay; if the dark activity is assumed distributed uniformly over the catalytic subunits, this requires $k_{cat} < 7\ s^{-1}$ (Arshavsky et al., 1992). Thus, saturating light causes ≥300-fold activation of the individual catalytic subunit.

Finally, it is noteworthy that for the intrinsic kinetic parameters $k_{cat} = 4{,}400\ s^{-1}$ and $K_m = 95$ μM, and for $[PDE^*]_{id} = [PDE^*]_{id} = 22$ μM, β_{max}/BP, the maximal rate constant for cGMP hydrolysis in the intact ROS divided by BP, the buffering power (Eq. 5), is 1,020 s^{-1}, or ~1,000 s^{-1}.

Previous Estimates of the Kinetic Parameters

Our results and analysis provide a plausible explanation for much of the variability in the literature in the estimates of the PDE K_m, since many experiments have been done with rod outer segments of varying degrees of structural integrity (for reviews, see Gillespie, 1990; Pugh and Lamb, 1993). Our results also point to at least three sources of variation in previous estimates of k_{cat}. The first is simply the difficulty of accurately estimating the total number of holo-PDEs. The second is the possibility of partially sealed outer segments, such as the electropermeabilized rods. The third is that the concentration of activating G-protein may have been too low in some cases (see Fig. 6).

Our results are not directly comparable to studies of PDE kinetic parameters in other species, nor to experiments in which PDE is activated with trypsinization (e.g., Sitaramayya et al., 1986). However, trypsin proteolysis disrupts outer segment structure, and thus is predicted by the theoretical analysis presented here to shift the K_m of disc stack preparations to lower values, independent of any direct effect of trypsin on the properties of the enzyme itself (see Pugh and Lamb, 1993).

Diffusion with Hydrolysis Explains the Apparent Light-dependence of K_m

The predicted effect of diffusion with hydrolysis within the disc stack is to cause an upward shift in the apparent K_m of the preparation, dependent on the size and integrity of disc stacks, and upon D_r, the radial diffusion coefficient. The theoretical analysis also shows that the magnitude of the K_m shift depends the degree to which PDE is activated. The dependence of apparent K_m on PDE activity can be understood

in terms of Eqs. 4 and 5 and Fig. 3: the greater the PDE activity level, the higher the value of the PDE rate constant (β in Eq. 5), and thus the smaller the radial space constant of decay of $[cGMP]_r$ from disc stack edge to disc stack center (Eq. 4). Fig. 8 shows calculations based on the model that illustrate the effect of increasing PDE activity: the predicted shift in K_m is a strongly increasing function of the fraction of PDE activated.

The predicted dependence of the apparent K_m on the fraction of PDE active provides a natural explanation of the light-induced increase in apparent K_m previously reported in ROS preparations having high structural integrity (Robinson et al., 1980; Kawamura and Murakami, 1988).

Further confirmation that diffusion with hydrolysis is responsible for the light-dependent K_m shift phenomenon, and not some other regulatory phenomenon of structurally intact ROS, is afforded by the cAMP data. The data show that the apparent K_m of cAMP is not affected by the degree of structural integrity. This lack of effect is expected on the basis of the diffusion with hydrolysis model (Fig. 4 *B*). For a rod of a given radius, the critical variable determining whether or not a shift occurs in an open disc stack preparation is the rate constant of hydrolysis (Eq. 5). Assuming that the kinetic parameters of the fully disrupted membranes are the intrinsic parameters of the PDE, we find from Table I that k_{cat}/K_m for cAMP is reduced almost 40-fold from that of cGMP. Cast in terms of Fig. 8, at substrate concentrations $\ll K_m$, changing the substrate from cGMP to cAMP is equivalent to reducing the fraction of active PDEs to ~2.5% the maximal value. Consistent with our interpretation, Kawamura and Murakami (1988) reported that no light-induced K_m increase occurred in ROS suspensions, either disrupted or intact, when cAMP is used as the reaction substrate.

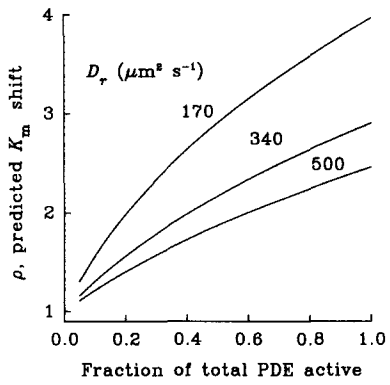

FIGURE 8. Dependence of the predicted K_m shift for cGMP of the open-stack model on fractional PDE activity and on D_r, the radial diffusion coefficient. Curves such as shown in Fig. 4 were generated for different fractions of PDE activity relative to the total, ranging from 0.05 to 1.0 in steps of 0.05; a K_m shift for each fraction of active PDE was then calculated (see Eq. 6), and the smooth curves in Fig. 8 were produced by interpolation. The calculations assumed the intrinsic kinetic parameters for cGMP to be k_{cat} = 4,400 s^{-1}, K_m = 95 μM, and they were performed for the three values of D_r indicated by the labels near the curves. As the fraction of PDEs active approaches 0, the predicted K_m shifts converge to 1 (i.e., no shift). Since increasing levels of light activation will necessarily increase the fraction of PDE active, the apparent K_m is predicted to increase as a function of light intensity. Note that K'_m, the apparent K_m, satisfies $K'_m = \rho K_m$, where ρ is the shift (Eq. 6).

Diffusion of cGMP in the ROS

For the fully open disc stack model to account for the approximate fourfold K_m shift of the small fragment preparation, it was necessary to assume that D_r, the radial diffusion coefficient of cGMP in the disc stacks, is 170 $\mu m^2 \cdot s^{-1}$. This value is about threefold reduced from the value D_{aq} = 500 $\mu m^2 \cdot s^{-1}$, expected for unhindered diffusion in an aqueous medium (see Lamb and Pugh, 1992). If in fact D_r = 170 $\mu m^2 \cdot s^{-1}$, the effective longitudinal diffusion coefficient for cGMP would be predicted to be $\sim$5 $\mu m^2 \cdot s^{-1}$ (Lamb and Pugh, 1992), which is within the range of current experimental evidence (Cameron and Pugh, 1990; Olson and Pugh, 1993). It seems possible that either weak binding or interdiscal structural features might cause a threefold reduction of D_r from D_{aq} (Olson and Pugh, 1993). The concentrations of cGMP used in the experiments reported here, however, are quite high relative to the affinity constants of known cGMP-binding sites, whose values lie in the range of 100 nM to 10 μM (Cote and Brunnock, 1993).

An alternative explanation to that requiring a threefold reduction of D_r from D_{aq} is that the path for diffusion of substrate into the disc stacks of the even the small-fragment preparation is more tortuous than that provided by the fully open-stack model (see Fig. 4). Indeed, it seems likely that such an increase in diffusional path length accounts for the shift of apparent K_m from the small- to large-fragment preparation. We cannot exclude the possibility that the average diffusional path in even the small-fragment preparation is greater than the rod radius. The virtue of the open-stack model is not that it provides a means of estimating D_r accurately, but rather, that it shows how the various parameters of the disc stack (disc radius and stack integrity) and of the PDE (fraction activation and intrinsic kinetic parameters of the substrate) can act to produce alterations in the apparent kinetic parameters.

The Electropermeabilized Rod Outer Segment

The electropermeabilized ROS has been developed as a preparation that provides access for small solutes to enter the cytosol, while preventing rapid loss of most soluble proteins (Gray-Keller et al., 1990). The evidence presented here helps to further characterize the electropermeabilized ROS membrane. The upper limit to cGMP influx at high $[cGMP]_{bulk}$ of $\sim 5 \times 10^7$ molecules$\cdot \mu m^2 \cdot s^{-1}$ supports the hypothesis that the "holes" in the membrane indeed behave somewhat like pores, through which only a limited number of molecules can pass per unit time. The permeability coefficient P_{cGMP} for cGMP of the electropermeabilized membrane of the electropermeabilized ROS (obtained at low $[cGMP]_{bulk}$) was estimated to be $\sim 1.6 \times 10^{-3}$ cm$\cdot s^{-1}$ (Appendix). This number can be related to a more familiar one, by virtue of the relation

$$P = \frac{D_{cG,mem}}{d}, \tag{10}$$

where $D_{cG,mem}$ is the diffusion coefficient for cGMP diffusing through the membrane, and d is the membrane thickness. Assuming a membrane thickness of 2.5 nm, we find $D_{cG,mem}$ = 0.03 $\mu m^2 \cdot s^{-1}$, >15,000-fold reduced from the value $D_{aq} \sim 500$ $\mu m^2 \cdot s^{-1}$ of the diffusion coefficient in an unhindered aqueous medium.

Amplification in Transduction Contributed by PDE

The dominant contributions to amplification in the activation phase of the G protein cascade of vertebrate photoreceptors are made by the two enzymatic steps, (*a*) the catalytic activation of G-protein by an individual Rh* and (*b*) the rate of hydrolysis of cGMP by an individual catalytic subunit of *PDE**. The contribution to amplification of an individual catalytic subunit can be shown to be proportional to the ratio $\frac{1}{2}k_{cat}/K_m$ (Lamb and Pugh, 1992; Pugh and Lamb, 1993), and our data provide a new, more secure estimate for this ratio in amphibian rods: $\frac{1}{2}k_{cat}/K_m \sim 2.3 \times 10^7$ $M^{-1} \cdot s^{-1}$.

Light Activation of PDE Diminished by Dilution

The data of Figs. 6 and 7 show that the activation of PDE by $G_{t\alpha}$ is diminished if the concentration of the suspension falls <4 μM rhodopsin in mechanically disrupted preparations and is restored by addition of $G_{t\alpha}$. This result is compatible with the observation of Yamazaki, Hayashi, Tatsumi, Bitensky, and George (1990) and Arshavsky et al. (1992), that washing ROS suspensions with GTP or GTPγS frees $\sim$70% of the $G_{t\alpha}$ present from the membrane. A recent report by Catty, Pfister, Bruckert, and Deterre (1992) has shown that interaction of bovine $G_{t\alpha}$ and PDE enhances anchoring of the complex to the membrane. This mechanism also shows cooperative behavior as a function of rhodopsin concentration.

While the data shown in Figs. 6 and 7 demonstrate how dilution of ROS membrane in the reaction cuvette <4 μM rhodopsin can diminish the recorded v_{max} of a fully light-activated system, they also point to a likely profound effect that would be expected at low light levels. Specifically, even when the cuvette contains 4 μM rhodopsin, if the fraction of rhodopsin isomerized is low, only a small fraction of $G_{t\alpha}$s produced is likely to bind and activate PDE (see Pugh and Lamb, 1993).

APPENDIX

Diffusion with Hydrolysis in the Disc Stack

This appendix presents the derivation of the relations used to characterize the effect of the rod disc stack and electropermeabilized rod outer segment on the apparent kinetic parameters of phosphodiesterase. A geometrical description of a disc stack segment is given in Fig. 3. An outline of the disc stack model has been presented in the body of the text; here, we will use the same notation.

The general assumption upon which our theoretical analysis rests is this: during the measurements of cGMP hydrolysis, the experimental system consists of two compartments in a steady-state relation. The first compartment is the bulk solution: fast, convective movements of cGMP occur in the bulk, keeping it well stirred; moreover, the bulk volume is so large that $[cGMP]_{bulk}$, the concentration of reaction substrate in the bulk, undergoes no significant change during the period of the experimental measurement. The second compartment is the open disc stack or permeabilized outer segment; cGMP can move in this compartment only by the relatively slow process of diffusion because of the very restricted dimensions of the interdiscal space.

The PDE hydrolysis reaction is assumed to take place entirely within the disc stacks; thus, we neglect the effect of the hydrolysis that occurs on the faces of discs that are directly in contact with the bulk solution. Such neglect will produce no more than 10% error, providing the disc stacks contain ≥ 10 discs, since in the case of a 10-disc stack, only 2 of 20 disc faces are exposed directly to the bulk.

Rod Outer Segment Disc Stack Fragments

We consider first the preparations in which completely open ROS disc stack fragments are suspended in the reaction cuvette. The partial differential equation governing diffusion with hydrolysis in a single interdiscal space is the following:

$$\frac{\partial[\text{cGMP}]}{\partial t} = D_r \nabla^2[\text{cGMP}] - \frac{[PDE^*]_{id} k_{cat}[\text{cGMP}]}{[\text{cGMP}] + K_m} \tag{11}$$

This equation expresses the local rate of change of [cGMP] in the disc stack as a sum of two terms: the first term is the rate due to diffusional flux; the second term is a loss term due to cGMP hydrolysis by PDE. The parameter D_r is the radial diffusion coefficient of the substrate, and ∇^2 is the Laplacian operator; because of the cylindrical symmetry of the ROS, the Laplacian operator is to be expressed in its cylindrical form, with no angular variation. Because the interdiscal space is extremely short relative to its radius, we can neglect the z-axis coordinate and express Eq. 11 in the radial and time coordinates only. For molecules the size of cGMP (or cAMP), the coefficient for diffusion in an unhindered aqueous medium is expected to be ~ 500 $\mu m^2 \cdot s^{-1}$ (Lamb and Pugh, 1992). The value of D_r is expected to be lower than the free aqueous diffusion coefficient because cGMP binding and possible physical hindrances imposed by structures in the stack.

In the general application of Eq. 11 $[PDE^*]_{id}$, the concentration of PDE^*s within the interdiscal space may be a function of time; however, because of the homogeneous light or $G_{t\alpha}$ activation, $[PDE^*]_{id}$ is not a function of r. In contrast, [cGMP], the concentration of cGMP within the stack, is a function of both time and the radial coordinate r, $0 < r \leq a$. The parameters k_{cat} and K_m have their usual meaning, with the understanding that the latter refers to the "true" or intrinsic Michaelis constant of an individual, fully active holo-PDE, and not necessarily to the apparent value measured in a particular experiment.

Steady-state Solution for [cGMP] $\ll K_m$

In characterizing the kinetic parameters of the PDE, we are interested in the steady-state condition; i.e., the condition $\partial[\text{cGMP}]/\partial t = 0$. It can be shown that when the bulk solution volume is much greater than the total interdiscal volume of the ROS fragments in suspension, steady-state conditions will be reached within a fraction of a second. Under steady-state conditions $[\text{cGMP}] = [\text{cGMP}]_r$; i.e., it is a function only of r, the radial coordinate. Moreover, $[\text{cGMP}]_r$ must decline steadily from the disc edge, $r = a$ to the disc center because of the hydrolysis that occurs. The rate of decline, however, will depend on the parameters of the disc stack in Eq. 11, and upon the boundary condition, $[\text{cGMP}]_{r=a} = [\text{cGMP}]_{bulk}$.

When the experimental conditions are such that $[cGMP]_{bulk} \ll K_m$, Eq. 11, the equation governing $[cGMP]_r$ in the steady-state becomes the homogenous Bessel equation:

$$0 = D_r \left[\frac{d^2[cGMP]}{dr^2} + \frac{1}{r} \frac{d[cGMP]}{dr} \right] - [PDE^*]_{id} k_{cat} [cGMP] \quad (12)$$

This equation admits an exact solution in terms of I_0, the modified Bessel function of order 0 (Carslaw and Jaeger, 1959):

$$\frac{[cGMP]_r}{[cGMP]_{bulk}} = \frac{I_0(r/\lambda_r)}{I_0(a/\lambda_r)}, \quad (13)$$

where as noted before, the boundary condition gives $[cGMP]_{r=a} = [cGMP]_{bulk}$. As described in the text (Eqs. 4 and 5), λ_r is the radial space constant of the decline of [cGMP] from the disc stack edge, determined by the disc stack parameters D_r, the radial diffusion coefficient of cGMP, and β, the rate constant of cGMP hydrolysis of the stack (Eq. 5). The distributions of $[cGMP]_r$ used to predict shifts in K_m (see Figs. 4 and 5) were computed with Eq. 13. The method of computing the shift in apparent K_m once $[cGMP]_r$ is known was described in the text (Eq. 6) and illustrated graphically in Fig. 4 (see also Fig. 8).

Eq. 13, in combination with Eqs. 6 and 7, can only be used to predict the rate of hydrolysis of the disc stack preparation for $[cGMP]_{bulk} \ll K_m$, and does not apply for arbitrary $[cGMP]_{bulk}$, as required by Eq. 3. Thus, Eq. 13 cannot be used to argue that the PDE velocity vs $[cGMP]_{bulk}$ curves for the open disc stack preparations should follow exactly the Michaelis curve over the whole range of $[cGMP]_{bulk}$. However, as we noted above, and it is seen in our data (Fig. 5 and Table I, k_{cat} data), diffusion with hydrolysis per se does not limit the maximum measurable enzyme velocity, provided that the bulk substrate concentration is raised sufficiently high. Thus, given that the region of the velocity vs substrate curves for which $[cGMP]_{bulk} \ll K_m$ is shifted by a single factor (Eq. 6), and that apparent v_{max} (or k_{cat}) is not dependent on the ROS fragment size, it is reasonable to characterize the complete velocity vs substrate curves of the ROS fragment preparations (Fig. 5) with the Michaelis saturation function, rather than solve the nonlinear Eq. 11, and compute v_{id} for each value of $[cGMP]_{bulk}$ (Eq. 3).

The Electropermeabilized Outer Segment

The steady-state kinetics of the PDE measured in the electropermeabilized ROS preparation exhibits two characteristic features, as seen in Fig. 5 and Table 1: (*a*) the v_{max} (or equivalently, apparent k_{cat}) is diminished, by about a factor of 2; (*b*) the apparent K_m for cGMP is shifted to a value, ~3 mM, that is very much higher than that of the disc stack fragment preparations (~400–500 μM). We now show that the apparent enzyme parameters of the electropermeabilized outer segment can be accounted for by an extension of the diffusion with hydrolysis model. The extended model shows that the permeability coefficient of the electropermeabilized membrane for cGMP is well defined, and that there is an upper limit, or maximum rate, at which cGMP can cross the permeabilized membrane.

When applied to the electropermeabilized ROS, the steady-state assumption requires that the net inward flux of cGMP across the permeabilized ROS membrane

must equal the total hydrolytic flux in the ROS. The total hydrolytic flux of cGMP, HF_{cGMP}, is given by

$$HF_{cGMP} = \tfrac{1}{2}\pi L[PDE^*]_{id}k_{cat}\int_0^a \frac{[cGMP]_r}{(cGMP]_r + K_m} 2rdr$$
$$= \frac{\tfrac{1}{2}\pi a^2 L\beta[cGMP]_{r=a}}{K'_m/K_m} \quad (14)$$

The first line of Eq. 14 is the integral of the local hydrolysis rate across the disc stack radius and over L, the length of the outer segment (see Eq. 3); the flux at the ends of the ROS is neglected. The second line in Eq. 14 applies only for $[cGMP]_r \ll K_m$, and is obtained by substitutions from Eqs. 4–7. In the case of the electropermeabilized ROS, we cannot assume $[cGMP]_{r=a} = [cGMP]_{bulk}$. Note that the cytosolic volume of the ROS is $V_{os} = \tfrac{1}{2}\pi a^2 L$, which is half of the envelope volume.

Upper Limit to Total cGMP Influx

Fig. 5 and Table I shows that the v_{max} of the electropermeabilized preparation saturates at a level that is ~50% that of the other preparations. Assuming the total complement of PDE is active, this result is interpreted in terms of the first line of Eq. 14 to mean that, regardless of how high $[cGMP]_{bulk}$ is raised, [cGMP] inside the ROS never rises sufficiently above the intrinsic K_m to produce a distribution $[cGMP]_r$ that saturates the *PDE**s with substrate across the disc stack. The maximal hydrolytic flux is readily computed from the maximal hydrolytic velocity or apparent k_{cat}, k'_{cat} = 2,000 s^{-1} (Table I): thus, the maximum hydrolytic flux is $[PDE^*]_{id}V_{os}N_{Av}k'_{cat} = 2.7 \times 10^{10}$ cGMP molecules·s^{-1}. Since at steady-state, the hydrolytic flux must equal to the net inward flux of cGMP, 2.7×10^{10} molecules·s^{-1} is also the maximum attainable net inward flux into an electropermeabilized ROS.

From the velocity vs $[cGMP]_{bulk}$ curve of the small fragment preparation (Fig. 5) one can read out $[cGMP]_{r=a}$, the marginal concentration in the electropermeabilized ROS at any $[cGMP]_{bulk}$; this follows, since by hypothesis $[cGMP]_{r=a} = [cGMP]_{bulk}$ for the small-fragment preparation, and there is no difference between the electropermeabilized ROS and the small fragments except for the distribution $[cGMP]_r$. In particular, by finding the intersection of a horizontal line corresponding to the maximal rate of hydrolysis of the electropermeabilized preparation with the curve for the small-fragment preparation, one can estimate $[cGMP]_{r=a}$ for the velocity-saturated, electropermeabilized ROS. More formally, one can invert the Michaelis expression characterizing the small-fragment preparation, solving for [cGMP], which produces a fractional rate of 2,000/4,400 for the small-fragment preparation whose apparent K_m is 380 μM (Table I). Thus, we find when its hydrolysis rate is saturated, in the electropermeabilized ROS $[cGMP]_{r=a} \sim 320$ μM.

Estimate of the Permeability Coefficient for cGMP

As we have just seen, at high levels of $[cGMP]_{bulk}$, the net inward flux of cGMP in the electropermeabilized ROS saturates. However, at sufficiently low levels of $[cGMP]_{bulk}$, the net diffusional flux DF_{cGMP} of cGMP across the electropermeabilized membrane is expected to obey Fick's First Law; i.e., it is expected to be proportional to the

difference in concentration across the membrane:

$$DF_{cGMP} = PA_{os}\{[cGMP]_{bulk} - [cGMP]_{r=a}\} \quad (15)$$

Here, $A_{os} \sim 2\pi aL$ is the area of the outer segment plasma membrane (say, in square centimeters), and P is the permeability coefficient (in $cm \cdot s^{-1}$). (For consistency of units, [cGMP] in Eqs. 14 and 15 should be expressed in molecules$\cdot cm^{-3}$.) To estimate the permeability coefficient and derive an expression for the ratio of $[cGMP]_{r=a}$ to $[cGMP]_{bulk}$, we equate the hydrolytic and diffusional fluxes of cGMP in Eqs. 14 and 15 to obtain by algebraic manipulation:

$$\frac{[cGMP]_{r=a}}{[cGMP]_{bulk}} = \frac{P}{P + \frac{\beta a}{4\rho}} \quad (16)$$

Eq. 16 expresses the concentration of cGMP just inside the plasma membrane of the electropermeabilized ROS in terms of $[cGMP]_{bulk}$, the known bulk substrate concentration; ρ, the K_m shift of the disc stack preparation (Eq. 6); β, the rate constant of hydrolysis in the ROS (Eq. 5); and P, the permeability coefficient of the electropermeabilized membrane for cGMP. Eq. 16 predicts that as P becomes very large, the electropermeabilized ROS will obey the same boundary condition as the open disc stack, viz. $[cGMP]_{r=a} = [cGMP]_{bulk}$.

To estimate P, we note that at its linear portion, the velocity vs substrate curve for the electropermeabilized preparation is shifted laterally a factor of ~ 16 from that of the small-fragment preparation. This shift factor gives the left-hand side of Eq. 16. (The lateral shift is about a factor or two larger than the shift in apparent K_m between the two preparations; however, it is the lateral shift of the linear portion of the curves that is relevant. This is because the reduced apparent k_{cat} of the electropermeabilized preparation, which results from the maximum cGMP influx limit, causes the apparent K_m to be $\sim 50\%$ lower than it would be were there no limit to the influx.) Thus, setting the left hand side of Eq. 16 to $1/16$, and inserting on the right-hand side the values $\beta = \beta_{max} = 1{,}000\ s^{-1}$, $a = 3 \times 10^{-4}$ cm, $\rho = 4.0$, we find $P = 1.25 \times 10^{-3}$ $cm \cdot s^{-1}$. Assuming the membrane thickness is $d = 2.5$ nm, this gives a diffusion coefficient for cGMP in the electropermeabilized membrane of $D_{mem,cGMP} = P\,d = 3 \times 10^{-10}\ cm^{-2}\ s^{-1}$, or $0.03\ \mu m^2\ s^{-1}$.

This work was supported by National Institutes of Health grants EY 00463 and EY 02660.

Original version received 14 September 1993 and accepted version received 26 January 1994.

REFERENCES

Arshavsky, V. Y., and M. D. Bownds. 1992. Regulation of deactivation of photoreceptor G-protein by its target enzyme and cGMP. *Nature.* 357:416–417.

Arshavsky, V. Y., C. L. Dumke, and M. D. Bownds. 1992. Non-catalytic cGMP binding sites of amphibian rod cGMP phosphodiesterase control interaction with its inhibitory γ-subunits. A putative regulatory mechanisms of the rod photoresponse. *Journal of Biological Chemistry.* 267: 24501–24507.

Barkdoll, III, A. E., E. N. Pugh Jr., and A. Sitaramayya. 1988. Kinetics of the hydrolysis of 8-bromo-cyclic GMP by the light-activated phosphodiesterase of toad rods. *Journal of Neurochemistry.* 50:839–846.

Biernbaum, M. S., and M. D. Bownds. 1985. Frog rod outer segments with attached inner segment ellipsoids as an in vivo model for photoreceptors on the retina. *Journal of General Physiology.* 85:83–105.

Bownds, D., A. Gordon-Walker, A.-C. Gaide-Huguenin, and W. Robinson. 1971. Characterization and analysis of frog photoreceptor membranes. *Journal of General Physiology.* 58:225–237.

Bradford, M. M. 1976. A rapid and sensitive method for the quantitation of microgram quantities of protein utilizing the principle of protein-dye binding. *Analytical Biochemistry.* 72:248–254.

Cameron, D. A., and E. N. Pugh, Jr. 1990. The magnitude, time course and spatial distribution of current induced in salamander rods by cyclic guanine nucleotides. *Journal of Physiology (London).* 430:419–439.

Carslaw, H. S., and J. C. Jaeger. 1959. Conduction of Heat in Solids. 2nd ed. Oxford University Press, Oxford.

Catty, P., C. Pfister, F. Bruckert, and P. Deterre. 1992. The cGMP phosphodiesterase—transducin complex of retinal rods. Membrane binding and subunits interactions. *Journal of Biological Chemistry.* 267:19489–19493.

Chabre, M., and P. Deterre. 1989. Molecular mechanism of visual transduction. *European Journal of Biochemistry.* 179:255–266.

Chumakov, K. M., M. N. Rozanov, and V. I. Agol. 1982. An RNA-dependent nucleoside triphosphate hydrolase from Krebs-II ascites tumor cells: detection and preliminary characterization. *European Journal of Biochemistry.* 127:309–314.

Cohen, A. I. 1971. Electron microscope observations of form changes in photoreceptor outer segments and their saccules in response to osmotic stress. *Journal of Cell Biology.* 48:547–565.

Cote, R. H., and M. A. Brunnock. 1993. Intracellular cGMP concentration in rod photoreceptors is regulated by binding to high and moderate affinity cGMP binding sites. *Journal of Biological Chemistry.* 268:17190–17198.

Dawis, S. M., R. M. Graeff, R. A. Heyman, T. F. Walseth and N. D. Goldberg. 1988. Regulation of cyclic GMP metabolism in toad photoreceptors. *Journal of Biological Chemistry.* 263:8771–8785.

Gillespie, P. G. 1990. Phosophodiesterases in visual transduction by rods and cones. *In* Cyclic Nucleotide Phosphodiesterases: Structure, Regulation and Drug Action. J. Beavo and M. D. Houslay, editors. John Wiley & Sons Ltd., Chichester, England. 163–184.

Gray-Keller, M. P., M. S. Biernbaum, and M. D. Bownds. 1990. Transducin activation in electropermeabilized frog rod outer segments is highly amplified, and a portion equivalent to phosphodiesterase remains membrane-bound. *Journal of Biological Chemistry.* 265:15323–15332.

Hamm, H. E., and M. D. Bownds. 1986. Protein complement of rod outer segments of frog retina. *Biochemistry.* 25:4512–4523.

Hurley, J. B., and L. Stryer. 1982. Purification and characterization of the gamma regulatory subunit of the cGMP phosphodiesterase from retinal rod outer segments. *Journal of Biological Chemistry.* 257:11094–11099.

Kawamura, S., and M. Murakami. 1986. Characterization of the light-induced increase in the Michaelis constant of the cGMP phosphodiesterase in frog rod outer segments. *Biochimica et Biophysica Acta.* 870:256–266.

Kawamura, S., and M. Murakami. 1988. Light-induced Michaelis constant increase is rapid and inherent in cGMP phosphodiesterase in frog rod outer segments. *Zoological Science.* 5:801–808.

Kincaid, R. L., and V. C. Manganiello. 1988. Assay of cyclic nucleotide phosphodiesterase using radiolabeled and fluorescent substrates. *Methods in Enzymology.* 159:457–470.

Korenbrot, J. I., D. T. Brown, and R. A. Cone. 1973. Membrane characteristics and osmotic behavior of isolated rod outer segments. *Journal of Cell Biology.* 56:389–398.

Lamb, T. D., P. A. McNaughton, and K.-W. Yau. 1981. Spatial spread of activation and background desensitization in toad rod outer segments. *Journal of Physiology (London).* 319:463–496.

Lamb, T. D., and E. N. Pugh, Jr. 1992. A quantitative account of the activation steps involved in phototransduction in amphibian photoreceptors. *Journal of Physiology.* 449:719–757.

Liebman, P. A., K. R. Parker, and E. A. Dratz. 1987. The molecular mechanism of visual excitation and its relation to the structure and composition of the rod outer segment. *Annual Review of Physiology.* 49:765–791.

McNaughton, P. A. 1990. Light response of vertebrate photoreceptors. *Physiological Reviews.* 70:847–884.

Miki, N., J. M. Baraban, J. J. Keirns, J. J. Boyce, and M. W. Bitensky. 1975. Purification and properties of the light-activated cyclic nucleotide phosphodiesterase of rod outer segments. *Journal of Biological Chemistry.* 250:6320–6327.

Olson, A., and E. N. Pugh, Jr. 1993. Diffusion coefficient of cyclic GMP in salamander rod outer segments estimated with two fluorescent probes. *Biophysical Journal.* 65:1335–1352.

Pugh, E. N., Jr., and T. D. Lamb. 1990. Cyclic GMP and calcium: The internal messengers of excitation and adaptation in vertebrate photoreceptors. *Vision Research.* 30:1923–1948.

Pugh, E. N., Jr., and T. D. Lamb. 1993. Amplification and kinetics of the activation steps in phototransduction. *Biochimica et Biophysica Acta (Bio-Energetics).* 1141:111–149.

Robinson, P. R., S. Kawamura, B. Abramson, and M. D. Bownds. 1980. Control of the cyclic GMP phosphodiesterase of frog photoreceptor membranes. *Journal of General Physiology.* 76:631–645.

Roof, D. J., and J. E. Heuser. 1982. Surfaces of rod photoreceptor disk membranes: integral membrane components. *Journal of Cell Biology.* 95:487–500.

Rosenkrantz, J. 1977. New aspects of the ultrastructure of frog rod outer segments. *International Review of Cytology.* 50:25–158.

Sidman, R. L. 1957. The structure and concentration of solids in photoreceptor cells studied by refractometry and interference microscopy. *Journal of Biophysical and Biochemical Cytology.* 3:15–30.

Sitaramayya, A., J. Harkness, J. H. Parkes, C. Gonzalez-Olivia, and P. A. Liebman. 1986. Kinetic studies suggest that light-activated cyclic GMP phosphodiesterase is a complex with G-protein subunits. *Biochemistry.* 25:651–656.

Stryer, L. 1991. Visual excitation and recovery. *Journal of Biological Chemistry.* 266:10711–10714.

Wensel, T. G., and L. Stryer. 1986. Reciprocal control of retinal rod cyclic GMP phosphodiesterase by its γ-subunit and transducin. *Proteins: Structure, Function and Genetics.* 1:90–99.

Wensel, T. G., and L. Stryer. 1990. Activation mechanism of retinal rod cyclic GMP phosphodiesterase probed by fluorescein-labeled inhibitory subunit. *Biochemistry.* 29:2155–2161.

Whalen, M. M., M. W. Bitensky, and D. J. Takemoto. 1990. The effect of the γ-subunit of the cyclic GMP phosphodiesterase of bovine and frog (*Rana catesbiana*) retinal rod outer segments on the kinetic parameters of the enzyme. *Biochemical Journal.* 265:655–658.

Woodruff, M. L., and M. D. Bownds. 1979. Amplitude, kinetics and reversibility of a light-induced decrease in guanosine 3′,5′-cyclic monophosphate in frog photoreceptor membranes. *Journal of General Physiology.* 73:629–653.

Yamazaki, A., F. Hayashi, M. Tatsumi, M. W. Bitensky, and J. S. George. 1990. Interactions between the subunits of transducin and cyclic GMP phosphodiesterase in Rana catesbiana rod photoreceptors. *Journal of Biological Chemistry.* 265:11539–11548.

Yee, R., and P. A. Liebman. 1978. Light-activated phosphodiesterase of the rod outer segment: kinetics and parameters of activation and deactivation. *Journal of Biological Chemistry.* 253:8902–8909.